

JAAS

Accepted Manuscript



This is an *Accepted Manuscript*, which has been through the Royal Society of Chemistry peer review process and has been accepted for publication.

Accepted Manuscripts are published online shortly after acceptance, before technical editing, formatting and proof reading. Using this free service, authors can make their results available to the community, in citable form, before we publish the edited article. We will replace this *Accepted Manuscript* with the edited and formatted *Advance Article* as soon as it is available.

You can find more information about *Accepted Manuscripts* in the [Information for Authors](#).

Please note that technical editing may introduce minor changes to the text and/or graphics, which may alter content. The journal's standard [Terms & Conditions](#) and the [Ethical guidelines](#) still apply. In no event shall the Royal Society of Chemistry be held responsible for any errors or omissions in this *Accepted Manuscript* or any consequences arising from the use of any information it contains.

1
2
3 1
4
5
6 2
7
8
9 3 **Transient signal isotope analysis using multicollecion of ion beams with**
10 4 **Faraday cups equipped with $10^{12} \Omega$ and $10^{11} \Omega$ feedback resistors.**
11
12
13 5
14
15
16 6
17
18 7
19

20 8 Alkiviadis Gourgiotis¹, Gérard Manhès¹, Pascale Louvat¹, Julien Moureau¹, Jérôme
21 9 Gaillardet¹
22
23
24

25 10
26 11
27 12 1. Institut de Physique du Globe de Paris, Sorbonne Paris Cité, Université Paris-Diderot,
28 13 UMR CNRS 7154, 1 rue Jussieu, 75238 Paris Cedex, France
29 14
30 15
31

32 16
33
34
35 17 **KEYWORDS**
36

37 18 Isotope ratio, transient signal, $10^{12} \Omega$ amplifiers, $10^{11} \Omega$, signal drift, signal attenuation,
38 19 hyphenation, chromatography, laser ablation, Faraday, MC-ICPMS, time lag
39
40
41
42 20
43
44 21
45
46
47 22
48
49 23
50
51
52 24
53
54 25
55
56
57 26
58
59
60

1
2
3 **Abstract**
4
5

6 To improve the precision of isotope analyses on low ion intensities using Faraday detection
7 system, amplifiers equipped with $10^{12} \Omega$ resistors (hereafter $10^{12} \Omega$ amplifiers) have been
8 developed. While the behavior of these amplifiers for steady signals has been well
9 investigated, there is not ample evidence regarding the use of $10^{12} \Omega$ amplifiers for transient
10 signal acquisition. In this work, we investigated the simultaneous use of amplifiers equipped
11 with $10^{12} \Omega$ and $10^{11} \Omega$ resistors for transient signal acquisition. Using the equation describing
12 the relationship between the input ion current and the output voltage in the amplifiers, we
13 showed how the transient signal duration influences the accuracy of the isotope ratio
14 measurements. In particular, lead transient signals were investigated using the Neptune Plus
15 MC-ICPMS and ^{204}Pb and ^{206}Pb isotopes were measured using $10^{12} \Omega$ and $10^{11} \Omega$ amplifiers,
16 respectively. $^{204}\text{Pb}/^{206}\text{Pb}$ isotope ratio showed an important drift due to the large time lag
17 between $10^{12} \Omega$ and $10^{11} \Omega$ amplifiers. The time lag was quantified (0.175(3) s) and the
18 isotopic drift was corrected using a method of internal signal synchronization. The $^{204}\text{Pb}/^{206}\text{Pb}$
19 drift corrected data obtained from the $10^{12} \Omega - 10^{11} \Omega$ amplifier configuration were compared
20 to the data obtained from $10^{11} \Omega - 10^{11} \Omega$ amplifiers. Our results point out that for low
21 transient signal intensities ($<10^{-13}$ A), the use of $10^{12} \Omega - 10^{11} \Omega$ amplifiers is more beneficial
22 in terms of isotope ratio uncertainty, repeatability and trueness, compared to the $10^{11} \Omega - 10^{11}$
23 Ω amplifier configuration.
24
25
26
27
28
29
30
31
32
33
34
35
36
37
38
39
40
41
42
43
44
45
46
47
48
49
50
51
52
53
54
55
56
57
58
59
60

1 Introduction

56

57 Transient signal isotope analysis using Multi Collection Inductively Coupled Plasma Mass
58 Spectrometry (MC-ICP MS) has become an emerging field in isotope analytical chemistry.
59 Various introduction systems have been coupled to the MC-ICPMS and the most commonly
60 used hyphenation techniques are: Laser Ablation (LA)¹, Liquid Chromatography (LC)^{2, 3}, Gas
61 Chromatography (GC)⁴ and Gold Trap (GT)⁵. The online coupling between these sample
62 introduction systems and the MC-ICPMS generates signals with time-dependent isotope
63 intensities. Transient isotope signals have durations varying generally from a few seconds to a
64 few minutes and isotope ratios must be accurately measured within these time windows.

65 Soon after the first appearance of hyphenated techniques between the MC-ICPMS and
66 different introduction systems, a systematic isotopic drift during isotope signal acquisition
67 was revealed^{1, 2, 4, 6-8}. For most transient signals, the amplifier's time response (time constant,
68 τ) is slow compared to the input ion signal time variation. However, the real cause of the
69 isotope drift is the short time lags between the time constants of the amplifiers involved in
70 Faraday multicollecion^{9, 10}. For transient signals with durations varying from a few seconds
71 to some minutes, the development of a new detection system with faster time response in
72 order to overcome the isotope ratio drift is not needed. Time response synchronization of
73 amplifiers equipped with $10^{11} \Omega$ feedback resistors, electronically or with post data treatment
74 methods⁹, can correct this drift.

75 Recently, measurements of low ion intensities have been extended using Faraday detection
76 systems with amplifiers equipped with $10^{12} \Omega$ resistors in the feedback loop¹¹ (10^{12} amplifiers
77 hereafter). While $10^{12} \Omega$ amplifiers provide 10 times higher voltage compared to $10^{11} \Omega$
78 amplifiers for a given ion beam, the noise level (Johnson noise) of the resistor only increases
79 by a factor of $\sqrt{10}$. Therefore, a theoretical 3-fold improvement in signal to noise ratio is
80 expected but in practice this ratio improves only by a factor of two¹². While most literature-
81 documented amplifiers using $10^{12} \Omega$ resistors are from Thermo Fisher Scientific, other
82 constructors propose similar developments¹³⁻¹⁵.

83

1
2
3 84 $10^{12} \Omega$ amplifiers have been successfully used in multicollection Thermal Ionisation Mass
4 Spectrometry (TIMS) and MC-ICPMS, either with $10^{12} \Omega$ amplifiers^{16, 17} only, or combined
5
6 85
7 86 with $10^{11} \Omega$ amplifiers¹⁸⁻²¹ or even with $10^{11} \Omega$ and $10^{10} \Omega$ amplifiers²².

8
9 87 Due to the quite slow time response, $10^{12} \Omega$ amplifiers have not yet been used for transient
10 signal acquisition. We present a first approach to evaluate the potential use of $10^{12} \Omega$
11
12 88
13 89 amplifiers for transient signal isotope analysis. Our study focuses on transient signal
14
15 90
16 91 theoretical large time shift ($\Delta t \sim 0.2$ s) between the isotope output signals. This work
17
18 92
19 93 investigates large transient signals (~ 50 s), with chromatographic peak shape, generated by a
20
21 94
22 Flow Injection system. Parameters like isotope ratio drift, uncertainty, repeatability and
23
24 95
25
26 96
27
28 97
29
30 98
31
32 99
33
34 100
35
36 101
37
38 102
39
40 103
41
42 104
43
44 105
45
46 106
47
48 107
49
50 108
51
52 109
53
54 110
55
56 111
57
58 112
59
60 113

2 Materials and methods

2.1 Instrumentation

100 The Neptune Plus MC-ICPMS (Thermo Scientific, Germany) used in this work has been
101 recently installed at the Institut de Physique du Globe de Paris (IPGP). The Neptune Plus
102 offers increased sensitivity due to a high performance interface pump combined with Jet-
103 sampler and H-skimmer cones. The detection system is equipped with ion counting systems
104 for small ion beams and ten Faraday cups; seven attached to amplifiers with $10^{11} \Omega$ resistors
105 (dynamic range from 0 to 50 V) and three attached to amplifiers with $10^{12} \Omega$ resistors
106 (recommended range < 0.1 V¹⁷). In this work, signals are reported relative to $10^{11} \Omega$ resistors.
107 All measurements were performed in static multi-collection mode with Faraday cups.
108 Thermo's virtual amplifier system²⁵ was used for assigning $10^{11} \Omega$ and $10^{12} \Omega$ amplifiers to
109 L1 cup (²⁰⁴Pb) (Table 2). The gains of the amplifiers were calibrated daily before the
110 analytical session and after each Faraday-amplifier re-assignment. The reproducibility of 10^{11}
111 Ω and $10^{12} \Omega$ amplifier gain was found to be better than 10 ppm per day. All amplifiers were
112 set for compensation of signal decay (*tau* correction) according to the procedure
113 recommended by the manufacturer²⁶. For lead isotope ratio measurements, although Hg is not
present in the standard solution, intensities of $m/q \sim 202$ were monitored for possible ²⁰⁴Hg
isobaric interference corrections and were found to be negligible ($< 10^{-4}$ V).

1
2
3 114 A Flow Injection system (FI) directly coupled to a tandem cyclone-Scott type spray chamber
4
5 115 SIS (Stable Introduction System, Thermo Scientific) with a PFA nebulizer (ESI, USA) was
6
7 116 used as the introduction system.

8
9 117 The flow injection system consists of a six-way high flow valve (FAST, ESI, USA) with an
10
11 118 injection loop of 2.4 μL and a peristaltic pump, which ensures the continuous flow of the
12
13 119 carrier solution (HNO_3 0.5 mol / L) at a rate of 50 $\mu\text{L min}^{-1}$. All signals were acquired with an
14
15 120 integration time of 0.5 s. Cup configuration for Pb measurements and MC-ICPMS operating
16
17 121 conditions are summarized in table 1 and 2.

18 122

19 123 **2.2 Reagents**

20 124

21
22
23
24 125 All sample dilutions were performed with 0.5 mol / L nitric acid obtained from sub-boiled 14
25
26 126 M nitric acid (EVAPOCLEAN system, Analab, France) and de-ionized water (Milli Q
27
28 127 system, Millipore, Milford, MA, USA). The same acid was also used as carrier solution for
29
30 128 the flow injection. For all Pb injections, the standard reference material SRM981 (NIST,
31
32 129 USA) was used. For the data treatment, the re-evaluated by Doucelance and Manhès²⁷ isotope
33
34 130 ratio values of the SRM981 were used: $^{208}\text{Pb}/^{206}\text{Pb} = 2.1681$, $^{207}\text{Pb}/^{206}\text{Pb} = 0.914970(17)$,
35
36 131 $^{204}\text{Pb}/^{206}\text{Pb} = 0.059019(5)$.

37 132

38 133 **3 Results and discussion**

39 134

40 135 **3.1 Evaluation of signal attenuation in amplifiers equipped with $10^{12} \Omega$ and $10^{11} \Omega$** 41 136 **resistors**

42
43
44 137 Figure 1 shows a simplified representation of the amplification circuit which is associated to
45
46 138 the Faraday cup of the Neptune MC-ICPMS. Each incoming singly charged positive ion is
47
48 139 neutralized with exactly one electron from the Faraday cup. The electron flux in the Faraday
49
50 140 cup is then converted to a voltage by an operational amplifier with a high-ohmic feedback
51
52 141 resistor. For instance, if using a $10^{11} \Omega$ feedback resistor, an entrance ion signal I of 10 pA
53
54 142 generates an output voltage V_{out} of 1 V.
55
56
57
58
59
60

1
2
3 143 Although amplifiers used by the Faraday cup detectors are stable over a wide range of
4 144 operating conditions, certain precautions must be met in order to achieve the desired pulse
5 145 response when a large feedback resistor is used. For this reason a capacitor is added around
6 146 the feedback resistor. This low-pass filter limits the bandwidth of the amplifier by attenuating
7 147 the input ion signals with frequencies higher than the cut-off frequency of the filter.

8
9
10
11 148 Signal attenuation through this circuit depends both on Resistor – Capacitor (RC) time
12 149 constant (τ) and on signal frequency.

13
14
15
16 150 The first order time constant ($\tau = RC$) for the Neptune's amplifier systems using $10^{11} \Omega$ and
17 151 $10^{12} \Omega$ resistors are ~ 0.1 s and ~ 0.3 s, respectively. In the case of transient signals generated
18 152 from hyphenation techniques described above, the signal frequency is expressed through the
19 153 time width of the signal.

20
21
22
23 154 Simultaneous use of $10^{11} \Omega$ and $10^{12} \Omega$ amplifiers for transient signal acquisition not only
24 155 generates an important isotope drift due to the large time lag⁹ ($\Delta\tau \sim 0.2$ s), but may also non-
25 156 uniformly attenuate signal intensities.

26
27
28
29 157 For studying the influence of the low-pass filter on transient signal attenuation, we need to
30 158 establish the relationship between the input ion current and the output voltage. We consider an
31 159 ideal operational amplifier (Figure 1) where I is the input ion current, I_1 and I_2 the currents
32 160 flowing into the capacitor and resistor, respectively. According to Kirchhoff's current law
33 161 $I = I_1 + I_2$. By replacing I_1 by $-CdV_{out}/dt$ and I_2 by $-V_{out}/R$, the relationship between the input ion
34 162 current and the output voltage can be obtained from the equation:

35
36
37
38
39
40 163

41
42
43 164
$$\frac{dV_{out}}{dt} = -\frac{1}{\tau}(IR + V_{out}) \quad (1)$$

44
45
46 165

47
48
49 166 where I , V_{out} , τ , R , are the input ion current, the output voltage, the amplifier first order time
50 167 constant ($\tau = RC$, C being the capacity) and the resistor, respectively. The negative sign
51 168 indicates that the inverting amplifier generates a 180° phase shift from the filter input to the
52 169 output.

1
2
3 170 In order to simulate an input ion transient signal (I) a Log-normal function (2) can be used.
4 171 The Log-normal function is a good approximation of the transient signals presented in this
5
6 172 work.
7

8
9 173

10
11
12 174
$$I(t) = h \times \text{Exp} \left[- \left(\text{Ln}(t / t^{apex}) / w \right)^2 \right] \quad (2)$$

13
14

15 175

16
17 176 where h , t^{apex} and w , are parameters corresponding to, amplitude, time of maximum signal and
18
19 177 peak width of the peak respectively.
20

21
22 178 Equation 1 was numerically solved for two time constants $\tau_{11}=0.1$ s and $\tau_{12}=0.3$ s,
23 179 (corresponding to 10^{11} Ω and 10^{12} Ω amplifiers, respectively), and for different peak widths
24
25 180 (w) of the input signal. The h and t^{apex} parameters of equation 2 have been kept constant. The
26
27 181 aim was to simulate signal attenuation as a function of the peak width (calculated at 10 % of
28
29 182 the signal I_{max}).
30

31 183 This calculation indicates how the signal attenuation in 10^{12} Ω and 10^{11} Ω amplifiers is related
32
33 184 to the transient signal width. It also defines the bias for the isotopic ratio calculated from the
34
35 185 attenuated output signals. Figure 2 illustrates the percentage of output signal attenuation
36
37 186 according to the peak width of the transient signal. The percentage of attenuation is calculated
38
39 187 as the ratio between the V_{out} maximum signal from equation 1 and the potential V obtained
40
41 188 from $I_{max}R$, where I_{max} is the maximum input ion intensity from equation 2 ($I_{max}R$ represents
42
43 189 the potential we should measure for a continuous ion signal with an intensity I_{max}).
44

45 190 For peak widths smaller than 10 s, the 10^{12} Ω amplifier strongly attenuates the output signal
46
47 191 compared to the 10^{11} Ω amplifier. In contrast, for peak widths larger than 40 s, signal
48
49 192 attenuations are significantly smaller. In the same figure, we also plot the ratios of the
50
51 193 attenuated signals for both 10^{12} Ω / 10^{11} Ω ($\Delta\tau = 0.2$ s) and 10^{11} Ω / 10^{11} Ω ($\Delta\tau = 0.006$ s)
52
53 194 amplifiers. It is obvious that for accurate isotope ratio measurements to be attained, signal
54
55 195 ratio attenuation between the amplifiers must be 1. For 10^{12} Ω - 10^{11} Ω amplifier
56
57 196 configuration, the isotopic bias is less than 10^{-3} for transient signal longer than 30 s (Figure 2).
58
59 197 In contrast, for the 10^{11} Ω - 10^{11} Ω amplifier configuration, the same isotopic bias is observed
60
198 for a transient signal longer than 3 s (Figure 2).

1
2
3 199 Consequently, the signal synchronization method which has been proposed in a recent work⁹,
4 200 corrects the isotopic drift due to the time lag between the amplifiers, but not the isotopic bias
5 201 due to non-uniform attenuation of the output signals. However, this approach is totally
6 202 effective, when taking into account the minimum durations of transient signals as defined
7
8 203 above.

11 204

14 205 **3.2 FI-MC-ICPMS transient signals with simultaneous use of 10^{11} Ω and 10^{12} Ω** 15 16 206 **amplifiers**

17
18 207 Lead transient signals were investigated using the Neptune Plus MC-ICPMS. The main
19 208 purpose was to explore the feasibility of simultaneous transient ion signal acquisition with
20 209 10^{11} Ω and 10^{12} Ω amplifiers and to compare the performances of 10^{11} Ω - 10^{11} Ω and 10^{12} Ω
21 210 - 10^{11} Ω amplifier configurations. Transient signals were generated with a flow injection
22 211 system in order to discount any possible isotope fractionation due to the introduction system
23 212 (LC, GC, LA...) and therefore to investigate the isotopic drifts coming from the time lag
24 213 between the amplifiers. Transient signals durations were adjusted to ~ 50 s (at 10 % of signal
25 214 max) (Fig. 3).

26
27 215 Ten independent injections of Pb SRM981 10 ng / g (ppb hereafter) were performed: five
28 216 using solely 10^{11} Ω amplifiers for all lead isotopes, and five with the Faraday cup of ^{204}Pb
29 217 isotope assigned to a 10^{12} Ω amplifier. All 10^{11} Ω amplifiers that have been chosen had
30 218 similar time responses ($\Delta\tau < 0.001$ s, isotopic drift \ll analytical precision) and only the
31 219 simultaneous use of 10^{11} Ω and 10^{12} Ω amplifiers presented an important time lag. The same
32 220 procedure was repeated for a 50 ppb concentration of Pb SRM981, in order to evaluate the
33 221 influence of higher signal intensities on 10^{12} Ω amplifiers.

34 222

35 223 Transient signal profiles at the same lead concentration were reproducible in peak-shape and
36 224 maximum intensity.

37 225

38 226 $^{208}\text{Pb}/^{206}\text{Pb}$, $^{207}\text{Pb}/^{206}\text{Pb}$ and $^{204}\text{Pb}/^{206}\text{Pb}$ isotope ratios were investigated and only the
39 227 $^{204}\text{Pb}/^{206}\text{Pb}$ ratio showed an important drift when ^{204}Pb Faraday cup was assigned to 10^{12} Ω
40 228 amplifier (Figure 3a and 3c). Raw point-by-point $^{204}\text{Pb}/^{206}\text{Pb}$ isotope ratios showed a
41 229 systematic increase of about 4 % with time over a period of ~ 30 s.

230 In the case where the ^{204}Pb isotope was detected with a $10^{11} \Omega$ amplifier no drift for the
231 $^{204}\text{Pb}/^{206}\text{Pb}$ ratio was observed (Figure 3b and 3d).

232 For the correction of the $^{204}\text{Pb}/^{206}\text{Pb}$ isotope ratio drift, the method of internal signal
233 synchronization was used⁹. The slope model was applied over a specific time zone (Fig.3,
234 segments within dashed lines) in which the measured isotope ratios showed a steady trend,
235 avoiding high isotope ratio noisy and spiky behavior (Fig. 3).

236 This zone corresponds to ^{204}Pb intensities higher than $\sim 2 \times 10^{-3} \text{ V}$ and $\sim 5 \times 10^{-3} \text{ V}$ for 10 ppb
237 and 50 ppb Pb SRM981, respectively. The same zone was used for the calculation of the
238 Relative Standard Deviation (RSD) for $^{204}\text{Pb}/^{206}\text{Pb}$ ratio. Signals of the $10^{12} \Omega$ amplifier are
239 reported relative to the intensity on the $10^{11} \Omega$ resistors.

240 After slope model minimization⁹, the time lag (time shift between ^{204}Pb and ^{206}Pb signals)
241 between the $10^{11} \Omega$ and $10^{12} \Omega$ amplifiers involved in ^{204}Pb and ^{206}Pb multi-collection was
242 found to be 0.174(18) s and 0.175(3) s for 10 ppb and 50 ppb SRM981 respectively.
243 Uncertainties were calculated as the standard deviation of the time lags obtained for five
244 injections and were expressed for a coverage factor $k = 2$. As expected, this time lag is much
245 higher compared to typical time lag values of $\sim 0.006 \text{ s}$ for $10^{11} \Omega$ amplifiers⁹.

246 The drift-corrected $^{204}\text{Pb}/^{206}\text{Pb}$ ratios were then calculated using the time lag values for each
247 injection, according to the method of internal signal synchronization⁹.

248 For low ^{204}Pb signals ($\sim 6 \times 10^{-3} \text{ V}$) the use of the $10^{12} \Omega$ amplifier after isotope drift correction
249 provides much more precise isotope ratio measurements compared to the $10^{11} \Omega$ amplifier.
250 The internal precision (% RSD) of the drift corrected $^{204}\text{Pb}/^{206}\text{Pb}$ ratios for the $10^{12} \Omega - 10^{11} \Omega$
251 configuration, was found to be three times better than the precision obtained using solely 10^{11}
252 Ω amplifiers (Fig. 3a and b). In contrast, % RSD of the drift uncorrected $^{204}\text{Pb}/^{206}\text{Pb}$ ratios
253 was similar to the % RSD for the $10^{11} \Omega - 10^{11} \Omega$ configuration.

254 For higher ^{204}Pb signals ($\sim 30 \times 10^{-3} \text{ V}$), quasi similar performances were achieved between the
255 drift corrected $10^{12} \Omega - 10^{11} \Omega$ and $10^{11} \Omega - 10^{11} \Omega$ amplifier configurations for $^{204}\text{Pb}/^{206}\text{Pb}$
256 isotope measurements in terms of internal precision. The % RSD on $^{204}\text{Pb}/^{206}\text{Pb}$ is however a
257 factor 1.5 better for the drift corrected ratios obtained for $10^{12} \Omega - 10^{11} \Omega$ amplifiers compared
258 to the ratios obtained for the $10^{11} \Omega - 10^{11} \Omega$ amplifier configuration (Fig. 3c and d).

1
2
3 259 In figure 4, $^{204}\text{Pb}/^{206}\text{Pb}$ ratios are plotted against $^{208}\text{Pb}/^{206}\text{Pb}$ ratios and compared to the
4
5 260 Exponential Mass Fractionation Law (EMFL). For these diagrams, the isotope ratios
6
7 261 contained within the dashed lines (Fig. 3) of the five injections are plotted together.

8
9 262 For 10 ppb Pb SRM981, the raw data for both $10^{12} \Omega - 10^{11} \Omega$ and $10^{11} \Omega - 10^{11} \Omega$ amplifier
10
11 263 configurations show random variations around the EMFL due to low ^{204}Pb signal (Fig. 4a and
12
13 264 b, grey points). In contrast, for 50 ppb Pb SRM981 the raw data of the $10^{12} \Omega - 10^{11} \Omega$
14
15 265 amplifier configuration follow a vertical straight line relative to the x -axis, crossing the EMFL
16
17 266 (Fig. 4c, grey points).

18
19 267 According to the model for the evolution of signal ratios during transient signals in a three
20
21 268 isotope plot, developed in a recent work⁹, this isotope ratio distribution clearly points out that
22
23 269 $\tau^{208}\text{Pb} = \tau^{206}\text{Pb} \neq \tau^{204}\text{Pb}$. Similarly, from figure 4d, it can be concluded that $\tau^{208}\text{Pb} = \tau^{206}\text{Pb} =$
24
25 270 $\tau^{204}\text{Pb}$. These observations are consistent with the time constants of the amplifiers which are
26
27 271 involved in both configurations for lead multi-collection. After $^{204}\text{Pb}/^{206}\text{Pb}$ drift correction
28
29 272 (for the $10^{12} \Omega - 10^{11} \Omega$ amplifier configuration) isotope ratios are in better agreement with
30
31 273 the EMFL (Fig. 4a and c, black points).

32
33 274

33 275 **3.3 Internal uncertainty, repeatability and trueness**

34
35 276

36
37 277 The isotope ratio uncertainty, trueness and repeatability of the base-line and mass
38
39 278 fractionation corrected $^{204}\text{Pb}/^{206}\text{Pb}$ ratios for both amplifier configurations, $10^{12} \Omega - 10^{11} \Omega$
40
41 279 and $10^{11} \Omega - 10^{11} \Omega$, were investigated. The instrumental mass fractionation was corrected
42
43 280 internally using the $^{208}\text{Pb}/^{206}\text{Pb}$ ratio of SRM981²⁷ and the exponential mass fractionation
44
45 281 law^{28, 29}.

46
47 282 The weighted mean and the weighted Standard Deviation (SD_w) of the $^{204}\text{Pb}/^{206}\text{Pb}$ ratios were
48
49 283 calculated for each independent injection using the following equations:

50
51 284

52
53
54 285
$$\overline{R_w} = \sum_{i=1}^n w_i R_i \quad (3)$$

$$SD_w = \sqrt{\sum_{i=1}^n w_i (R_i - \bar{R}_w)^2} \quad (4)$$

287

288 where, w_i are the normalized weights calculated on the basis of the point by point ^{208}Pb
289 signals, \bar{R}_w and R_i the weighted $^{204}\text{Pb}/^{206}\text{Pb}$ ratio mean and the point by point base line and
290 mass fractionation corrected $^{204}\text{Pb}/^{206}\text{Pb}$ ratios, respectively. For all calculations, only isotope
291 ratios contained within dashed lines (Fig. 3) were considered. In table 3, the $^{204}\text{Pb}/^{206}\text{Pb}$ ratio
292 uncertainty is expressed through the weighted Standard Deviation while the repeatability is
293 the % RSD of the five injections. Trueness is expressed as the difference between the average
294 ratio for the five injections and the reference $^{204}\text{Pb}/^{206}\text{Pb}$ value²⁷.

295

296 The results clearly show that in order to benefit from the full performance range of the
297 Faraday multi-collectors when involving $10^{12} \Omega$ and $10^{11} \Omega$ amplifiers, isotope signal
298 synchronization for drift correction is important (Table 3).

299

300 For 10 ppb SRM981 the drift corrected data point out that the $10^{12} \Omega - 10^{11} \Omega$ configuration
301 provides 2.6 and 1.7 times lower $^{204}\text{Pb}/^{206}\text{Pb}$ ratio uncertainties and repeatability, respectively,
302 compared to the results provided from the $10^{11} \Omega - 10^{11} \Omega$ configuration (Fig. 5, table 3). For
303 higher ^{204}Pb signals (50 ppb SRM981) uncertainties obtained by both $10^{12} \Omega - 10^{11} \Omega$ (drift
304 corrected data) and $10^{11} \Omega - 10^{11} \Omega$ amplifier configurations are quasi similar. In contrast,
305 repeatability was improved by a factor four when using $10^{12} \Omega - 10^{11} \Omega$ amplifiers.

306 Moreover, drift corrected ratios of the $10^{12} \Omega - 10^{11} \Omega$ configuration showed better
307 performances in terms of ratio trueness compared to the $10^{11} \Omega - 10^{11} \Omega$ configuration for
308 both 10 ppb and 50 ppb SRM981.

309

310 At this point we are interested to assess whether the slight $^{204}\text{Pb}/^{206}\text{Pb}$ ratio trueness bias
311 observed when using the $10^{12} \Omega - 10^{11} \Omega$ configuration is related to the non-uniform signal
312 attenuation. When $10^{12} \Omega - 10^{11} \Omega$ amplifiers are involved in multicollection, the theoretical
313 ratio of attenuated signals for peak widths of about 50 s is ~ 0.99972 (Fig.2) which generates a

1
2
3 314 trueness bias of about ~ -0.028 %. Trueness of the drift corrected $^{204}\text{Pb}/^{206}\text{Pb}$ ratios for 50 ppb
4 315 SRM981 may be explained by this non-uniform signal attenuation (Table 3). In order to test
5 316 this hypothesis, continuous signal analysis was performed and similar $^{204}\text{Pb}/^{206}\text{Pb}$ ratio
6 317 trueness bias was observed. Moreover, trueness ratio biases were observed for the $10^{11} \Omega$ -
7
8 $10^{11} \Omega$ amplifiers which have similar time responses (Table 3). Therefore, we believe that this
9 318 slight trueness biases are not related to the non-uniform signal attenuation. However, trueness
10 319 variations are much smaller than the corrected isotope ratio uncertainty, and are therefore not
11 320 significant.
12 321
13
14
15
16

322

323 4 Conclusion

324

325 In this work, we considered the simultaneous use of $10^{12} \Omega$ and $10^{11} \Omega$ amplifiers in
326 multicollection for isotope transient signal detection. We demonstrated that $10^{12} \Omega$ amplifiers
327 can be used for transient signal acquisition despite their slow time response compared to the
328 $10^{11} \Omega$ amplifiers. We evaluated how the signal attenuation in $10^{12} \Omega$ and $10^{11} \Omega$ amplifiers is
329 related to the transient signal width. We quantified the bias for the isotopic ratio resulting
330 from the non-uniformly attenuated output signals. This isotopic bias cannot be corrected with
331 the method of internal signal synchronization⁹. However, this method is effective for transient
332 signal with durations longer than 30 s, providing accuracies better than 0.1 % for the drift
333 corrected ratios.

334 This approach has been applied in lead transient signals of a width of ~ 50 s. As expected, the
335 large time lag between $10^{12} \Omega$ and $10^{11} \Omega$ amplifiers generated an important isotopic drift
336 which was successfully corrected using the method of internal signal synchronization⁹. The
337 drift corrected data showed that for low intensity transient signals ($<10^{-13}$ A), the use of 10^{12}
338 Ω - $10^{11} \Omega$ amplifiers is more beneficial in terms of isotope ratio uncertainty, repeatability and
339 trueness, compared to the $10^{11} \Omega$ - $10^{11} \Omega$ amplifier configuration. For higher signals ($\sim 3 \times 10^{-13}$
340 A), isotope ratio uncertainties obtained by both configurations are similar while
341 repeatability and trueness continue to be better for $10^{12} \Omega$ - $10^{11} \Omega$ configuration. It would be
342 interesting in a future work, to examine the non-uniform signal attenuation in a $10^{13} \Omega$ - 10^{12}
343 Ω - $10^{11} \Omega$ amplifier configuration³⁰ for isotope transient signals with distinct durations.

1
2
3 344 Finally, we believe that the use of $10^{12} \Omega$ amplifiers for transient signal acquisition opens up
4 345 new possibilities for the on-line isotope analysis techniques of small sample sizes.

6
7 346 It should be noted that as the method of peak area integration eliminates the artifacts due to
8 347 the time shift between two transient signals (isotope signals not in phase), it is relevant for
9 348 transient signal measurements. In addition, this method is effective regardless of the transient
10 349 signal duration.

11
12 350

13
14
15 351 For transient signals with duration higher than 30 s and when both $10^{12} \Omega$ and $10^{11} \Omega$
16 352 amplifiers are used, the method of peak integration and the method of signal synchronization
17 353 applied in this work provide similar isotope ratio trueness and repeatability.

18
19 354

20
21 355 However, the ease of implementation differs for the two methods.

22
23 356

24
25 357 For the peak area integration method, the area to be integrated is a function of the desired
26 358 measured isotope accuracy. For example, for an accuracy of 0.1%, more than 99.9% of the
27 359 peak area has to be integrated.

28
29 360

30
31 361 In the case where both $10^{12} \Omega$ and $10^{11} \Omega$ amplifiers are used, for 99.9 % of peak area
32 362 integration the integrated peak areas of the isotope signals are not defined by the same time
33 363 intervals (beginning and end of peak integration) due to the important time shift between the
34 364 isotope signals. The method of peak area integration thus becomes tricky when measurement
35 365 accuracy better than 0.1 % is required and necessitates a detailed analysis of the signal profile
36 366 in the near-baseline areas where the signal to noise ratio is quite low.

37
38 367

39
40 368 On the contrary, the method of signal synchronization does not depend on the integrated peak
41 369 area, and can thus be applied to time intervals easily identified by a high signal to noise ratio
42 370 (e.g. 70 % - 90% of the isotopic signal), regardless of the near-baseline peak areas.

43
44 371

45
46 372

47
48 373

49
50 374

1
2
3 375 **Acknowledgements**
4

5 376 We would like to warmly thank Jean-Louis Birck and Anastassios Skarlatos for many helpful
6 377 discussions on detection systems. Parts of this work were supported by IPGP
7
8 378 multidisciplinary program PARI, and by Paris–IdF region SESAME Grant no. 12015908.
9
10

11 379

12
13 380

14
15
16 381

17
18
19 382

20
21 383

22
23 384

24
25
26 385

27
28
29 386

30
31 387

32
33 388

34
35
36 389

37
38 390

39
40
41 391

42
43 392

44
45
46 393

47
48 394

49
50 395

51
52 396

53
54
55 397
56
57
58
59
60

398 **References**

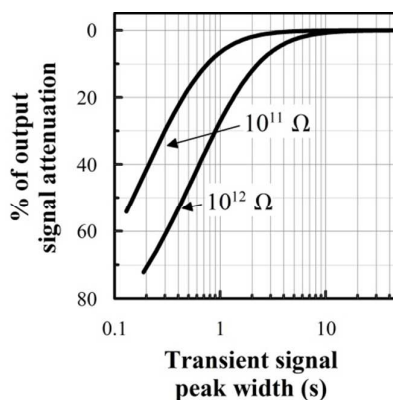
- 399 1. T. Hirata, Y. Hayano and T. Ohno, *Journal of Analytical Atomic Spectrometry*, 2003, **18**, 1283-
400 1288. DOI: 10.1039/b305127g.
- 401 2. I. Gunther-Leopold, J. K. Waldis, B. Wernli and Z. Kopajtic, *International Journal of Mass*
402 *Spectrometry*, 2005, **242**, 197-202.
- 403 3. F. Gueguen, H. Isnard, A. Nonell, L. Vio, T. Vercoouter and F. Chartier, *Journal of Analytical*
404 *Atomic Spectrometry*, 2015, **30**, 443-452. DOI: 10.1039/c4ja00361f.
- 405 4. E. A. Krupp and O. F. X. Donard, *International Journal of Mass Spectrometry*, 2005, **242**, 233-
406 242. DOI: 10.1016/j.ijms.2004.11.026.
- 407 5. R. D. Evans, H. Hintelmann and P. J. Dillon, *Journal of Analytical Atomic Spectrometry*, 2001,
408 **16**, 1064-1069. DOI: 10.1039/b103247j.
- 409 6. I. Gunther-Leopold, B. Wernli, Z. Kopajtic and D. Gunther, *Analytical and Bioanalytical*
410 *Chemistry*, 2004, **378**, 241-249. DOI: 10.1007/s00216-003-2226-1.
- 411 7. M. Dzurko, D. Foucher and H. Hintelmann, *Analytical and Bioanalytical Chemistry*, 2009, **393**,
412 345-355.
- 413 8. E. M. Krupp, C. Pecheyran, S. Meffan-Main and O. F. X. Donard, *Analytical and Bioanalytical*
414 *Chemistry*, 2004, **378**, 250-255. DOI: 10.1007/s00216-003-2328-9.
- 415 9. A. Gourgiotis, S. Berail, P. Louvat, H. Isnard, J. Moureau, A. Nonell, G. Manhes, J.-L. Birck, J.
416 Gaillardet, C. Pecheyran, F. Chartier and O. F. X. Donard, *Journal of Analytical Atomic Spectrometry*,
417 2014, **29**, 1607-1617. DOI: 10.1039/c4ja00118d.
- 418 10. T. Pettke, F. Oberli, A. Audetat, U. Wiechert, C. R. Harris and C. A. Heinrich, *Journal of*
419 *Analytical Atomic Spectrometry*, 2011, **26**, 475-492. DOI: 10.1039/c0ja00140f.
- 420 11. D. Tuttas, J. Schwieters, N. Quaas and C. Bouman, *Improvements in TIMS High Precision*
421 *Isotope Ratio Measurements for Small Sample Sizes*, Thermo Fisher Scientific, Bremen, Germany,
422 *Technical note 30136*, 2007.
- 423 12. M. E. Wieser and J. B. Schwieters, *International Journal of Mass Spectrometry*, 2005, **242**, 97-
424 115. DOI: <http://dx.doi.org/10.1016/j.ijms.2004.11.029>.
- 425 13. T. R. Ireland, N. Schram, P. Holden, P. Lanc, J. Ávila, R. Armstrong, Y. Amelin, A. Latimore, D.
426 Corrigan, S. Clement, J. J. Foster and W. Compston, *International Journal of Mass Spectrometry*, 2014,
427 **359**, 26-37. DOI: <http://dx.doi.org/10.1016/j.ijms.2013.12.020>.
- 428 14. Z. Palacz, D. Wanless, I. Turner and T. Jones, *Comparative analytical performance of $1e^{11} \Omega$*
429 *and $1T (1e^{12} \Omega)$ resistors on Phoenix TIMS demonstrated using NBS U500 uranium standard*, *Technical*
430 *Brief T10812, IsotopX, UK*.
- 431 15. High precision 10 ng Lithium samples, *Application note AN34*, nu plasma II. DOI:
432 <http://www.nu-ins.com/wp-content/uploads/AN34-NPII-Lithium.pdf>.
- 433 16. A. Makishima and E. Nakamura, *Journal of Analytical Atomic Spectrometry*, 2012, **27**, 891-
434 895. DOI: 10.1039/c2ja10337k.
- 435 17. J. M. Koornneef, C. Bouman, J. B. Schwieters and G. R. Davies, *Journal of Analytical Atomic*
436 *Spectrometry*, 2013, **28**, 749-754. DOI: 10.1039/c3ja30326h.
- 437 18. A. Makishima and E. Nakamura, *Journal of Analytical Atomic Spectrometry*, 2010, **25**, 1712-
438 1716. DOI: 10.1039/c0ja00015a.
- 439 19. S. Richter, H. Kuhn, Y. Aregbe, M. Hedberg, J. Horta-Domenech, K. Mayer, E. Zuleger, S.
440 Burger, S. Boulyga, A. Kopf, J. Poths and K. Mathew, *Journal of Analytical Atomic Spectrometry*, 2011,
441 **26**, 550-564. DOI: 10.1039/c0ja00173b.
- 442 20. J. Liu and D. G. Pearson, *Chemical Geology*, 2014, **363**, 301-311. DOI:
443 <http://dx.doi.org/10.1016/j.chemgeo.2013.11.008>.
- 444 21. Q. Chang, J.-I. Kimura and B. S. Vaglarov, *Journal of Analytical Atomic Spectrometry*, 2015, **30**,
445 515-524. DOI: 10.1039/c4ja00297k.
- 446 22. M. Schiller, C. Paton and M. Bizzarro, *Journal of Analytical Atomic Spectrometry*, 2012, **27**, 38-
447 49. DOI: 10.1039/c1ja10272a.

- 1
2
3 448 23. A. Menditto, M. Patriarca and B. Magnusson, *Accred Qual Assur*, 2007, **12**, 45-47. DOI:
4 449 10.1007/s00769-006-0191-z.
5 450 24. Joint Committee for Guides in Metrology, *International vocabulary of metrology - Basic and*
6 451 *general concepts and associated terms (VIM)*. 2012.
7 452 25. H. Lerche and J. B. Schwieters, *US Pat. 6472659 B1*, Thermo Electron (Bremen), issued
8 453 29/10/2002.
9 454 26. A. Trinquier, C. Bouman and N. L. Schwieters, *10¹² Ω amplifiers for high precision isotope ratio*
10 455 *measurements of small sample sizes*, Thermo Fisher Scientific, Bremen, Germany, Technical note
11 456 30249, 2013.
12 457 27. R. Doucelance and G. Manhès, *Chemical Geology*, 2001, **176**, 361-377. DOI:
13 458 [http://dx.doi.org/10.1016/S0009-2541\(00\)00409-5](http://dx.doi.org/10.1016/S0009-2541(00)00409-5).
14 459 28. W. A. Russell, D. A. Papanastassiou and T. A. Tombrello, *Geochimica et Cosmochimica Acta*,
15 460 1978, **42**, 1075-1090. DOI: [http://dx.doi.org/10.1016/0016-7037\(78\)90105-9](http://dx.doi.org/10.1016/0016-7037(78)90105-9).
16 461 29. C. N. Maréchal, P. Télouk and F. Albarède, *Chemical Geology*, 1999, **156**, 251-273. DOI:
17 462 [http://dx.doi.org/10.1016/S0009-2541\(98\)00191-0](http://dx.doi.org/10.1016/S0009-2541(98)00191-0).
18 463 30. J. M. Koornneef, C. Bouman, J. B. Schwieters and G. R. Davies, *Analytica Chimica Acta*, 2014,
19 464 **819**, 49-55. DOI: <http://dx.doi.org/10.1016/j.aca.2014.02.007>.

22 465

24 466

Graphical abstract



This work is a first attempt to evaluate the potential use of $10^{12} \Omega$ amplifiers for transient signal isotope analysis and we show for the first time how the transient signal duration influences the accuracy of the isotope ratio measurements.

MC-ICPMS conditions

Sample Introduction System

Nebulizer	PFA Micro-Concentric (ESI)
Spray chamber	tandem Cyclone-Scott (SIS)
Sample gas (L min^{-1})	1
Liquid uptake ($\mu\text{L min}^{-1}$)	50
Cones	Jet-sampler and H-skimmer

MC-ICPMS conditions

RF power (W)	1200
Plasma gas flow rate (L min^{-1})	15
Auxiliary flow rate (L min^{-1})	1.3
Resolution	Low (400)
Integration time (s)	0.524
Sensitivity on ^{208}Pb (V ppm^{-1} , continuous introduction mode)	40

Table 1. MC-ICPMS operating conditions

Cup configuration	L3	L1	H1	H2	H3
Amplifiers	$10^{11} \Omega$	$10^{12} \Omega/10^{11} \Omega$	$10^{11} \Omega$	$10^{11} \Omega$	$10^{11} \Omega$
Isotopes	^{202}Hg	^{204}Pb	^{206}Pb	^{207}Pb	^{208}Pb

Table 2. Cup and amplifier configuration

$^{204}\text{Pb}/^{206}\text{Pb}$	$10^{12} \Omega - 10^{11} \Omega$ Amp		$10^{11} \Omega - 10^{11} \Omega$ Amp
	Drift uncorrected	Drift corrected	
10 ppb SRM981			
Average ratio	0.059113	0.059056	0.058965
% Uncertainty	2.19	0.98	2.54
% Repeatability	0.47	0.23	0.4
% Trueness	0.159	0.063	-0.092
50 ppb SRM981			
Average ratio	0.059089	0.058999	0.058980
% Uncertainty	2.33	0.35	0.53
% Repeatability	0.084	0.028	0.111
% Trueness	0.118	-0.034	-0.066

Table 3. 10 ppb and 50 ppb SRM981 average $^{204}\text{Pb}/^{206}\text{Pb}$ values for five injections of: isotope ratio, uncertainty, repeatability and trueness for both drift uncorrected and drift corrected isotope ratios. Ratio uncertainty is expressed through the average value of the weighted Standard Deviation for five injections while the repeatability is the % RSD of the five $^{204}\text{Pb}/^{206}\text{Pb}$ ratio values. Trueness is expressed as the difference between the average ratio for the five injections and the reference $^{204}\text{Pb}/^{206}\text{Pb}$ value. Uncertainty and repeatability are expressed for a coverage factor $k = 2$. The reference $^{204}\text{Pb}/^{206}\text{Pb}$ value was re-evaluated by Doucelance and Manhès²⁶ and is equal to 0.059019(5).

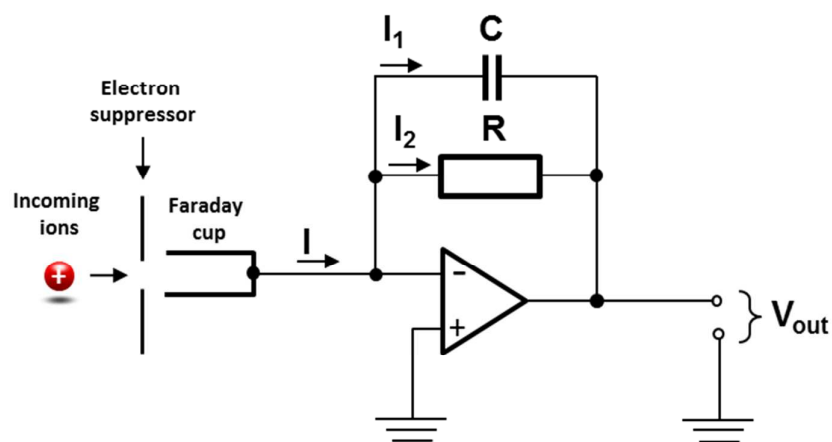


Figure 1. Schematic circuit diagram of Faraday cup detection system. Where C , R and I are the dumping capacity, the high ohmic feedback resistor and the input ion current, respectively. From the Kirchhoff's current law we obtain $I = I_1 + I_2$. Where I_1 and I_2 are the currents flowing into the capacitor and resistor, respectively.

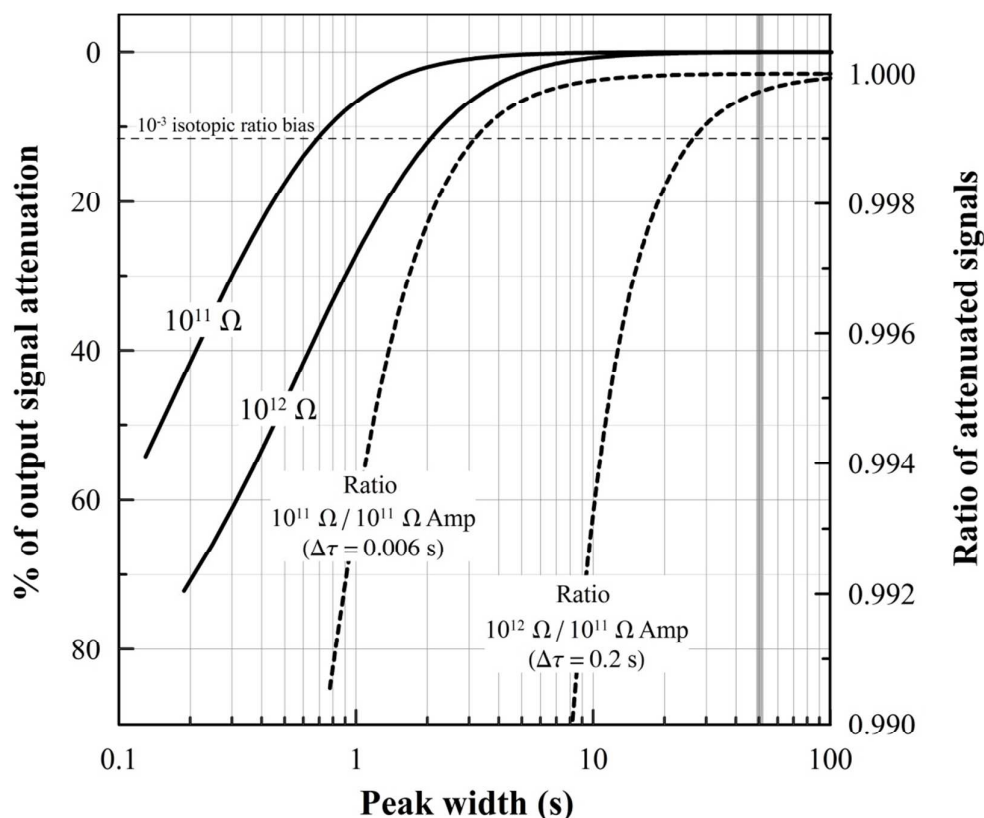


Figure 2. Percentage of output signal attenuation (solid lines) and ratio of attenuated signals (dashed lines) as a function of transient peak width. The ratio of attenuated signals was calculated by dividing directly: 1) the 10¹² Ω to 10¹¹ Ω output signal attenuations considering a time lag of 0.2 s and 2) the 10¹¹ Ω to 10¹¹ Ω output signal attenuations considering a time lag of 0.006 s. Shaded area corresponds to the peak widths of this work (~50 s). Horizontal dashed line represents the 0.999 value for the ratio of attenuated signals.

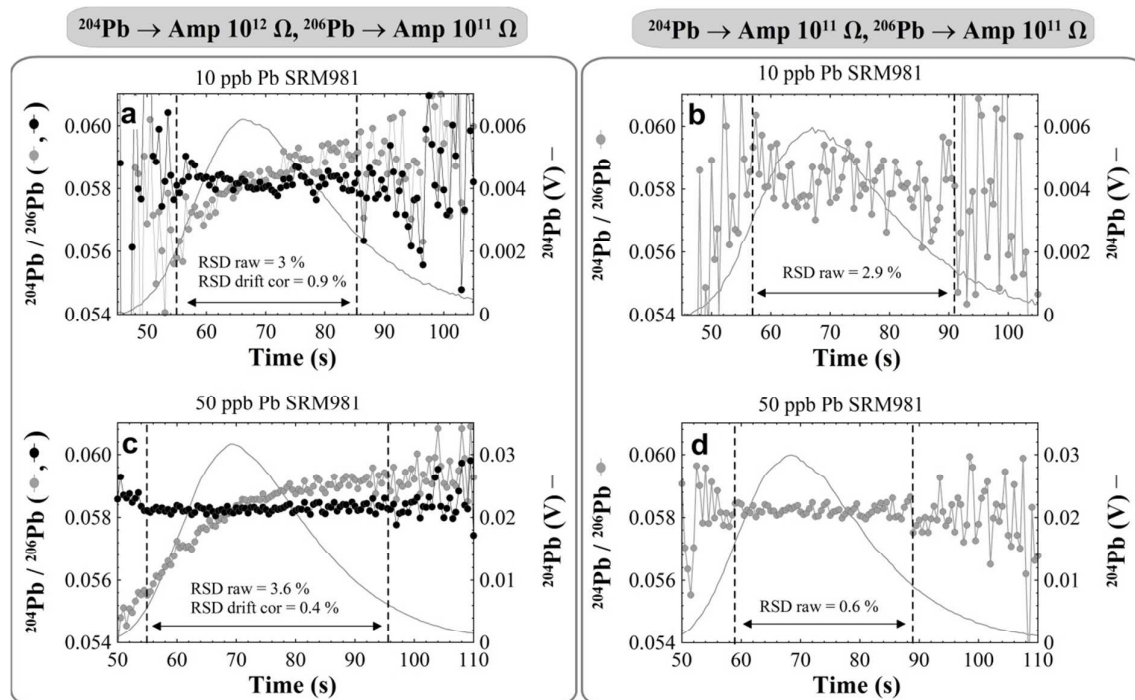


Figure 3. Lead transient signals using a flow injection system directly coupled to the Neptune Plus. For $^{204}\text{Pb}/^{206}\text{Pb}$ ratio acquisition, $10^{12} \Omega - 10^{11} \Omega$ amplifier configuration (on the left side, a and c) and $10^{11} \Omega - 10^{11} \Omega$ amplifier configuration (on the right side, b and d), were respectively used. Grey and black points correspond to raw and drift corrected data, respectively. No isotopic drift was observed for the $10^{11} \Omega - 10^{11} \Omega$ amplifier configuration due to similar amplifier time constants. For all calculations (isotope ratio value, RSD, uncertainty, repeatability, trueness) the zone within the dashed lines was considered.

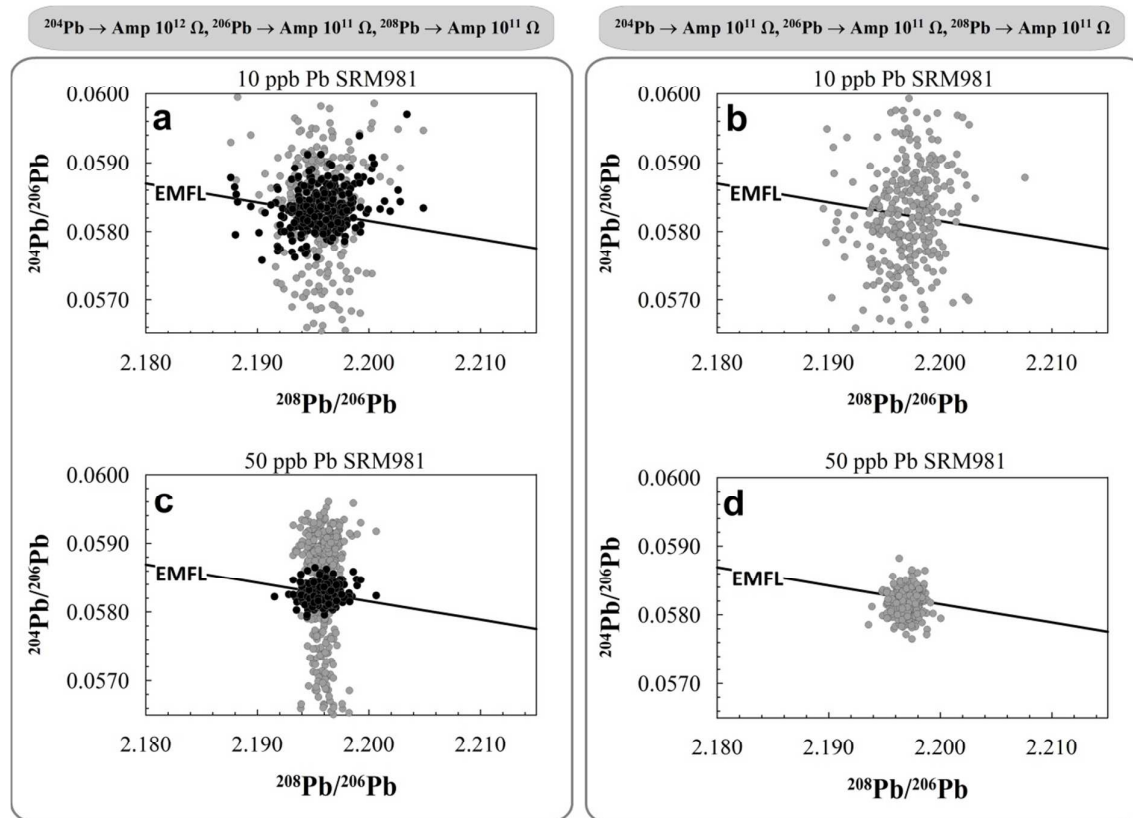


Figure 4. Three isotope plots for lead transient signals with a flow injection system directly coupled to the Neptune Plus. For $^{204}\text{Pb}/^{206}\text{Pb}$ ratio acquisition, $10^{12} \Omega$ - $10^{11} \Omega$ amplifier configuration (on the left side, a and c) and $10^{11} \Omega$ - $10^{11} \Omega$ amplifier configuration (on the right side, b and d), were respectively used. For $^{208}\text{Pb}/^{206}\text{Pb}$ ratio acquisition, $10^{11} \Omega$ - $10^{11} \Omega$ amplifier configuration was used. Grey and black points correspond to raw and drift corrected data, respectively and the straight line to the Exponential Mass Fractionation Law (EMFL).

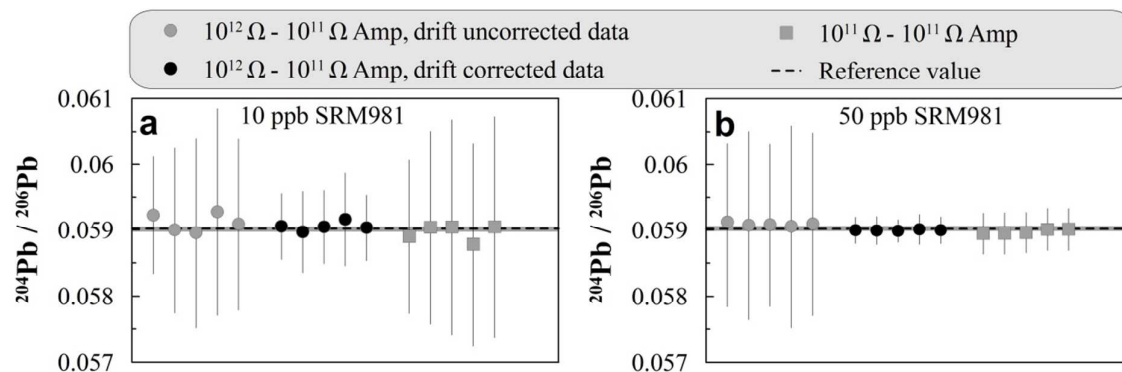


Figure 5. Flow injection - MC-ICPMS base line-corrected and mass fractionation-corrected $^{204}\text{Pb}/^{206}\text{Pb}$ ratios for 10 ppb SRM981 (a) and 50 ppb SRM981 (b). Dashed lines represent reference value of $^{204}\text{Pb}/^{206}\text{Pb}$ isotope ratio for the SRM981 standard solution and the shaded areas correspond to the reference value uncertainty (2σ). All isotope ratio uncertainties are expressed for a coverage factor $k=2$.